Original Article

JCBFM

Journal of Cerebral Blood Flow & Metabolism
2020, Vol. 40(2) 263–275

DOI: 10.1177/0271678X18822921
journals.sagepub.com/home/jcbfm

Impaired meningeal lymphatic vessel development worsens stroke outcome

Pavel Yanev[1,*], Katherine Poinsatte[1,*], Devon Hominick[2], Noor Khurana[2], Kielen R Zuurbier[1], Marcus Berndt[1], Erik J Plautz[1], Michael T Dellinger[2,3,*] and Ann M Stowe[1,4,*]

Abstract

The discovery of meningeal lymphatic vessels (LVs) has sparked interest in identifying their role in diseases of the central nervous system. Similar to peripheral LVs, meningeal LVs depend on vascular endothelial growth factor receptor-3 (VEGFR3) signaling for development. Here we characterize the effect of stroke on meningeal LVs, and the impact of meningeal lymphatic hypoplasia on post-stroke outcomes. We show that photothrombosis (PT), but not transient middle cerebral artery occlusion (tMCAo), induces meningeal lymphangiogenesis in young male C57Bl/J6 mice. We also show that *Vegfr3*$^{wt/mut}$ mice develop significantly fewer meningeal LVs than *Vegfr3*$^{wt/wt}$ mice. Again, meningeal lymphangiogenesis occurs in the alymphatic zone lateral to the sagittal sinus only after PT-induced stroke in *Vegfr3*$^{wt/wt}$ mice. Interestingly, *Vegfr3*$^{wt/mut}$ mice develop larger stroke volumes than *Vegfr3*$^{wt/wt}$ mice after tMCAo, but not after PT. Our results reveal differences between PT and tMCAo models of stroke and underscore the need to consider method of stroke induction when investigating the role of meningeal lymphatics. Taken together, our data indicate that ischemic injury can induce the growth of meningeal LVs and that the absence of these LVs can impact post-stroke outcomes.

Keywords

Stroke, meningeal lymphatics, lymphangiogenesis, VEGFR3

Received 22 June 2018; Revised 13 November 2018; Accepted 26 November 2018

Introduction

Lymphatic vessels (LVs) perform several important physiological functions. LVs absorb intestinal lipids, transport immune cells, and return fluid and macromolecules to the blood vasculature.[1] LVs are present in most tissues in the body and were recently observed in the meninges.[2,3] The meninges consist of three distinct membranes (dura, arachnoid, and pia matter) that cover the brain and spinal cord. Meningeal LVs are located in the dura mater and run adjacent to the sagittal sinus, transverse sinus, middle meningeal arteries, and the retroglenoid veins.[2,3] Functional studies with mice revealed that these LVs transport cerebrospinal fluid (CSF) and brain interstitial fluid to the cervical lymph nodes.[2–4] Though meningeal LVs were only recently characterized, substantial progress has been made in describing the development of these LVs.

The murine meningeal lymphatic network begins to develop just before birth and is fully developed by postnatal day 28.[5] Similar to peripheral LVs, meningeal LVs depend on vascular endothelial growth factor receptor-3 (VEGFR3) signaling for their development.[5,6] VEGFR3 is a receptor tyrosine kinase that is activated by VEGF-C and VEGF-D.[7,8] VEGF-C heterozygous mice and K14-VEGFR3-Ig transgenic mice

[1]Department of Neurology and Neurotherapeutics, University of Texas Southwestern Medical Center, Dallas, TX, USA
[2]Hamon Center for Therapeutic Oncology Research, University of Texas Southwestern Medical Center, Dallas, TX, USA
[3]Division of Surgical Oncology, Department of Surgery, University of Texas Southwestern Medical Center, Dallas, TX, USA
[4]Department of Neurology, University of Kentucky, Lexington, KY, USA
[*]These authors contributed equally to this work.

Corresponding authors:
Michael T Dellinger, Department of Surgery, University of Texas Southwestern Medical Center, 6000 Harry Hines Blvd, Dallas, TX 75390-8593, USA.
Email: Michael.Dellinger@utsouthwestern.edu
Ann M Stowe, Department of Neurology, BBSRB 363 University of Kentucky, 741 S Limestone St., Lexington, KY 40536-0509, USA.
Email: Ann.Stowe@uky.edu

exhibit a hypoplastic network of meningeal LVs.[3,5] Additionally, deletion of VEGF-C or VEGFR3 during early postnatal life impairs the development of meningeal LVs.[5] Interestingly, deletion of VEGFR3 in adult mice causes meningeal LVs to regress.[5] Therefore, VEGFR3 signaling is required for the development and maintenance of meningeal LVs. Importantly, mice that exhibit meningeal lymphatic hypoplasia could be used to determine whether meningeal LVs play a role in the pathophysiology of diseases of the central nervous system, such as stroke.

Our understanding of the relationship between LVs and stroke is limited. One report found that the level of VEGF-C in the brain increased after the focal stroke model of photothrombosis (PT).[9] Another report found that surgical ligation of cervical LVs exacerbated cerebral edema and increased infarct size after transient middle cerebral artery occlusion (tMCAo).[10] This finding suggests that meningeal lymphatic drainage plays a role in the pathophysiology of stroke. However, there are no direct studies exploring the relationship between meningeal LVs and stroke. In the present study, we utilize two different stroke models (PT and tMCAo) to determine whether stroke affects meningeal LVs, and whether dysfunctional meningeal LVs impact post-stroke outcomes.

Materials and methods

Animals

All animal experiments were performed in accordance with an animal protocol (2016-101640) approved by the Institutional Animal Care and Use Committee of University of Texas Southwestern Medical Center in accordance with AAALAC accreditation and current PHS Animal Welfare Assurance requirements. All animal reporting complies with ARRIVE guidelines. Adult male C57Bl/6 mice were purchased from an on-campus supplier (6–10 weeks old). Prox1-tdTomato mice were maintained on a C57Bl/6 background and *Vegfr3*$^{wt/wt}$ and *Vegfr3*$^{wt/mut}$ mice[6] were maintained on a C3H genetic background. All animals were group-housed under standard conditions (food and water provided ad libitum, 12-h light cycle) with standard cob bedding. Mice were randomized to sham/experimental groups and all experimenters were blinded to condition (e.g. surgery, genotype) for data acquisition and analyses.

Photothrombotic stroke

Mice were anesthetized with isoflurane (4% induction, ~2% maintenance,70% NO_2/ 30%O_2); VetEquip V-1 system, Piny River, VA, USA), then placed in a stereotaxic frame (David Kopf Instruments, Tujunga, CA, USA), with surgeons blinded to condition. Body temperature was maintained at ~37°C with a warming pad (Kent Scientific, Torrington, CT, USA), ophthalmic ointment was applied to eyes, and anesthetic depth was assessed via breathing rate and absence of reflexes (corneal, toe pinch). After shaving and disinfecting (betadine and alcohol) the skin, the target region was exposed using a midline incision (~1 cm) in the scalp, blunt dissection of underlying connective tissues, and bone drying using hydrogen peroxide and/or cotton-tipped applicators. Analgesia was provided locally (at incision) using lidocaine and systemically using buprenorphine (0.05 mg/kg sq). Rose Bengal (5 mg/ml in saline, 40 mg/kg ip) was injected 1 min prior to laser activation. A green-light laser (Coherent Sapphire, Santa Clara, CA, USA; 561 nm; 2.7 mm collimated beam diameter) was aimed at the target coordinates (right hemisphere, AP 0.0, ML 1.7) using minimal power prior to Rose Bengal injection, then activated at 45 mW (calibrated at skull position prior to surgery) for 15 min to produce the stroke. Following stroke induction, the incision was closed with 6–0 nylon suture, and saline administered (0.2 ml sq) for fluid replacement. Mice recovered in a heated (30°C) chamber until ambulatory, then returned to their home cage. Sham mice received a midline scalp incision and Rose Bengal injection but were not exposed to the laser. A total of $n = 27$ mice were included for all PT stroke surgeries, with complete survival and no exclusions.

tMCAo

tMCAo was performed as previously described,[11–13] with minor modifications, by surgeons blinded to condition. Briefly, animals were anesthetized (2% isoflurane/ 70% NO_2/ 30%O_2) and kept warm on a heating pad at 37°C. A small incision was made to pull the muscle back from the skull and reveal the middle cerebral artery (MCA) for Doppler flowmetry. To induce a transient occlusion, an intra-luminal suture was inserted into the common carotid artery (CCA) to block blood flow into the MCA. A transcranial Laser Doppler (Moor Instruments, Wilmington, DE, USA) was used to detect successful MCA occlusion, defined as a greater than 80% reduction in blood flow compared to baseline value. The occlusion duration was 60 min, during which time mice were allowed to recover in a 34°C incubator. Mice were then re-anesthetized and continued occlusion confirmed by Doppler. The occluding suture was then removed. A successfully reperfused MCA was defined as one that returned to more than 50% initial blood flow. Sham mice underwent all surgical preparations and permanent CCA ligation, but in the absence of intra-luminal suture

placement. Neurological deficit was tested 15 min following reperfusion. Mice were rated on a scale of 0–4 with 0 being no observable change in behavior and 4 being severe impairments in moving spontaneously.[14] Animals were monitored until they fully recovered, and daily thereafter while remaining in standard cage housing with moistened chow available. Mice that did not meet both occlusion and reperfusion criteria were removed from the study, which included, out of $n = 34$ mice, $n = 3$ failed occlusion, $n = 3$ failed reperfusion, and 1 post-operative death.

Whole-mount staining of meninges

Meninges were fixed overnight in 4% paraformaldehyde while still attached to the skullcap. Skullcaps were then incubated in ethanol/acetone for 20 min at −20°C and then the meninges were carefully dissected away from the skullcap. Meninges were washed with PBS and then blocked overnight with PBS + 0.3% TX-100 + 20% Aquablock (East Coast Bio, North Berwick, ME, USA). Primary antibody was then added and the meninges were incubated overnight at 4°C. The following primary antibodies were used: rat anti-CD31 (1:1000; eBiosciences, San Diego, CA, USA), goat anti-Lyve-1 (1:1000; R&D Systems, Minneapolis, MN, USA), hamster anti-podoplanin (1:1000; Abcam, San Francisco, CA, USA), and rabbit anti-Prox1 (1:500; AngioBioCo, Del Mar, CA, USA). Tissues were washed with PBS + 0.3% TX-100 and then incubated overnight at 4°C with the appropriate secondary antibodies. Tissues were washed again with PBS + 0.3% TX-100, placed on slides, and coverslips were mounted with ProLong Gold (Thermo Fisher Scientific, Waltham, MA, USA) anti-fade reagent.

TissueCyte

A single Prox1-tdTomato brain was assessed using 3D serial two-photon tomography (STPT)[15] of the entire brain volume (TissueCyte 1000 microscope, TissueVision, Cambridge, MA). On the day of imaging, an agarose block containing the brain was attached to a custom magnetic slide on a magnetized stage within the imaging chamber. STPT imaging is a block-face imaging technique in which two-dimensional (2D) mosaic images in the coronal plane are formed near the cut surface of the brain (within ~100 μm of the surface), followed by physical sectioning with a built-in vibrating microtome to cut away the imaged tissue, preparing a new cut surface for imaging.[15] Individual tiles were adjusted via flat-field correction and stitched into 2D mosaic images of each imaging plane via custom software (“AutoStitcher,” TissueVision) and saved to network-attached storage drives.

Histology

Animals were sacrificed, by an overdose of isoflurane and brains were perfused with 20 ml PBS followed by 40 ml of 4% paraformaldehyde in 0.1 mol/L phosphate buffer, pH 7.4. Extracted brains were cryoprotected by immersion in 15% sucrose (for 48 h) and 30% sucrose solutions (for 48 h). Coronal sections (30 μm) were cut on a freezing microtome. Sections were rinsed, blocked (10% NGS, 0.2% Triton, 10 mM PBS), washed (0.2% FSG, 10 mM PBS) and exposed to antibodies (Ab) for NeuN 1:100 (Sigma, St. Louis, MO, USA) overnight at 4°C. Day 2, sections were washed, blocked, and secondary Ab (Invitrogen, Waltham, MA, USA; 1:300) applied. Standard cresyl violet stain was used to identify pyknotic neurons in coronal sections and alkaline phosphatase used to stain vessels.[16] Infarct and lateral ventricle volumes were quantified by a blinded observer. Infarct volumes were corrected for cavitation by normalizing to the contralesional hemisphere.[17,18] Four mice from the tMCAo cohort (1 *Vegfr3*$^{wt/wt}$ and 3 *Vegfr3*$^{wt/mut}$) had no discernible infarct identified by histology and were thus excluded from final infarct and lateral ventricle volume analysis.

Rotarod testing

Mice were trained on the Rotarod task for 11 days prior to stroke, ensuring they reached a stable baseline performance. Mice were tested on postoperative days 2, 7 and 14 to determine motor impairment. The equipment, as well as the testing surface, was cleaned with dilute alcohol prior to testing each animal. The investigator conducting and scoring the behavioral tests was blinded to the experimental assignment of the animals. For rotarod testing, mice were placed on a Rotamex rotarod apparatus (Columbus Instruments, Columbus, OH, USA), facing away from the experimenter. The rod initially rotated at 2 r/min and then accelerated at a rate of 1 r/min/5 s until the mice fell off the rod or 300 s passed. The time to falling off or the first “spin,” where the mouse completed a full rotation holding on to the rod, was considered the end of the trial. Mice received four trials per day with a 15-min inter-trial interval. The scores at −1 and −4 days were averaged and this value was defined as baseline. Performance at 2, 7, and 14 days post-stroke was normalized to baseline and all values are presented as percent of baseline. The four mice above, with no discernible infarcts, were not included in final analyses.

Stereology

DNA-binding, neuron-specific protein NeuN (neuronal nuclei) contained in the nucleus and the nucleolus of the neuron was used to identify cells, which were

counted using the same stereological parameters (such as sampling fractions and counting unit) as in the Alk-Phos-stained vessel branching point counts. The optical fractionator design was used to estimate the neuron and vessel branching point numbers (N) in each region of interest (ROI).[19] Each ROI was systematically, uniformly and randomly sampled in the section plane (the x-y plane) and across the thickness of the sections (the z-axis), superimposing a grid of three-dimensional optical dissectors on top on the acquired multilayer NanoZoomer image. Pilot estimated sampling parameters of the probe to count at approximately 900–1200 NeuN positive cells and 200–250 vessel branching points per studied ROI were sufficient to obtain Gundersen coefficient of error (CE) below 0.07 and 0.1, respectfully. To calculate the total number of microvessels (w), we counted the total number for each anastomosis (n) and marked each type of anastomosis with a different marker that indicates the valence (v) of the anastomosis, corresponding to the number of vessels it splits into:[20] $w = 1 + \sum [(v-2)/2]n$. We estimated the density of neurons and microvessels dividing the numbers obtained with the optical fractionator by the volume of each region as calculated by Cavalieri's principle.

Lymphatic vessel index measurements

To quantify meningeal LVs, we took two 10× images of each meningeal sample as previously described.[21] One image was taken of LVs at the sagittal sinus and the other image was taken of the area to the right of sagittal sinus, over the right sensorimotor cortex (region for analysis shown in Figure 1(a)) Images were opened in ImageJ and a grid (2500 cm^2) was placed over the images. The number of gridlines that intersected on LVs was counted and reported as the LVI for the sample. Some animals were excluded due to rips in the meninges that precluded reliable LVI measurements.

Statistical analysis

Statistical analysis was performed using GraphPad Prism 5.0 from data analyzed by blinded experimenters. Normal distribution was not assumed, so non-parametric tests

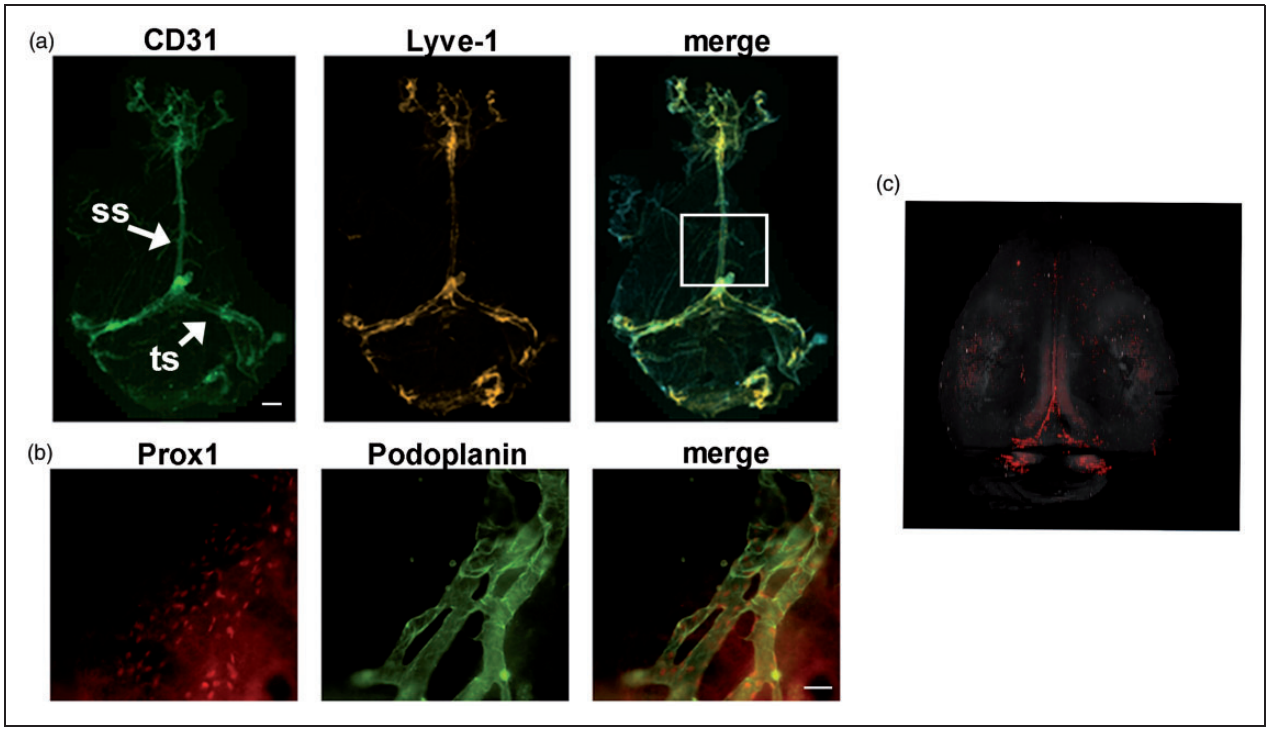

Figure 1. Whole mount imaging of meningeal lymphatic vessels in mice. (a) Meningeal LVs were characterized by whole-mount immunofluorescence staining for CD31 (green) and Lyve-1 (red). Low magnification view of meningeal LVs. LVs run alongside the sagittal sinus (ss) and transverse sinus (ts). The boxed regions in panel A outline the areas that we analyzed in our stroke experiments to acquire lymphatic vessel index (LVI) at the ss. (b) Representative images showing Prox1 (red) and podoplanin (green) expression by meningeal LVs around the transverse sinus (TS). (c) A 3D rendering of meningeal LVs (red) in a Prox1-tdTomato transgenic mouse was generated using serial two-photon tomography. The signal from the hippocampus was digitally removed. (a), scale bar is 1000 μm; (b), scale bar is 20 μm.

were used. Infarct volumes, meningeal LVs, microvessel density, neuronal counts, were compared using a two-tailed Mann–Whitney test. Differences in ventricle volumes and rotarod performance were compared using a repeated measure two-way ANOVA with Sidak post hoc. Correlations between ventricle volume and infarct volume were analyzed using a linear regression. Power analyses were based on prior infarct volume data and used to estimate sample size, with a power of 0.8 and α of 0.05. Post hoc analyses after surgical or histological exclusions showed a power of 100% for groups vs. sham conditions. For *Vegfr3*$^{wt/wt}$ /*Vegfr3*$^{wt/mut}$ studies, the tMCAo cohort final power was 75%, while the PT cohort was powered at 20%. Results were plotted with GraphPad Prism 5.0, as means with error bars representing standard deviations.

Results

The meningeal LV network does not extend into the parenchyma

To confirm that the meninges have LVs, we collected meninges and performed whole-mount immunofluorescence staining with antibodies against CD31, Lyve-1, Podoplanin, and Prox1. CD31 is a marker of blood and lymphatic endothelial cells,[22] whereas Lyve-1, Podoplanin, and Prox1 are markers of lymphatic endothelial cells.[23–25] Meningeal LVs were located next to the sagittal and transverse sinuses and expressed Lyve-1, Podoplanin, Prox1, and CD31 (Figure 1). These results confirm that the meninges have LVs and show that these LVs can be identified by whole-mount immunofluorescence staining. Two-photon serial tomography was performed to generate a 3D rendering of the LV network in the meninges of Prox1-tdTomato mice, which possess endogenously fluorescent LVs. Prox1-tdTomato mice exhibited tdTomato^{+} meningeal LVs (Figure 2), and tdTomato^{+} neurons/cells in the hippocampus. Importantly, this whole brain imaging showed LVs were limited to the meninges as no intraparechymal LVs were present.

Meningeal lymphangiogenesis occurs after PT

Two weeks after PT, mice had an average infarct volume of $6.1 \pm 2.7\,mm^3$ (Figure 3(a)). To determine the effect of PT on meningeal LVs, we measured the meningeal lymphatic vessel index (LVI) in PT and sham animals. The LVI at the sagittal sinus was significantly higher in PT mice (84.6 ± 18) than sham mice (24.8 ± 6.24; Figure 3(c)). Interestingly, LVs sprouted from the sagittal sinus into the alymphatic zone over the right sensorimotor cortex (Figure 3(b) and (d)) corresponding to the anatomical area where the stroke occurred. This area lacked LVs in sham animals, showing that PT stroke induces meningeal lymphangiogenesis.

Meningeal lymphangiogenesis was not detected after tMCAo

Two weeks after tMCAo, mice had an average infarct volume of $34.6 \pm 15.2\,mm^3$ (Figure 4(a)). In contrast to PT stroke which produced focal occlusions in the sensorimotor cortex, infarcts in mice after tMCAo were more variable, with ischemic tissue detected in both cortical and subcortical areas. To determine the effect of tMCAo on meningeal LVs, we measured the meningeal LVI in tMCAo and sham animals (Figure 4(b) to (d)). The LVI at the sagittal sinus was not significantly different between tMCAo (54.4 ± 11.3) and sham (42.2 ± 9.7) animals. It should be noted, however, that the sham tMCAo group exhibited higher LVI vs. PT sham ($p < 0.05$), potentially secondary to permanent CCA ligation. Additionally, the right sensorimotor cortex remained alymphatic in tMCAo (0 ± 0) and sham (0 ± 0) mice. These results indicate that no detectable meningeal lymphangiogenesis occurs after tMCAo.

VEGFR3 signaling controls the development of meningeal LVs

VEGFR3 signaling controls the development of LVs,[5] and *Vegfr3*$^{wt/mut}$ mice are heterozygous for a point mutation in the kinase domain of VEGFR3. This mutation impairs the kinase activity of VEGFR3 and exerts a dominant-negative effect on VEGFR3 signaling.[6,26] We found that *Vegfr3*$^{wt/mut}$ mice have fewer meningeal lymphatics than *Vegfr3*$^{wt/wt}$ mice (Figure 5). Importantly, the density of microvessels and the number of neurons in the sensorimotor cortex and in the striatum were not significantly different between *Vegfr3*$^{wt/wt}$ and *Vegfr3*$^{wt/mut}$ mice (Figure 5(c) and (d)). Therefore, the development of meningeal LVs, but not the development of blood vessels or neurons, is affected in *Vegfr3*$^{wt/mut}$ mice.

Meningeal lymphatic hypoplasia does not affect infarct volumes or outcomes after PT

Vegfr3$^{wt/mut}$ mice have a hypoplastic network of meningeal LVs that can be used to determine whether meningeal LVs affect infarct and ventricle volumes, and recovery after stroke. Two weeks after PT, infarct volumes were not significantly different between *Vegfr3*$^{wt/wt}$ ($4.5 \pm 3.1\,mm^3$) and *Vegfr3*$^{wt/mut}$ ($6.0 \pm 2.9\,mm^3$) mice ($p = 0.31$; Figure 6(a)). The meningeal LVI at the sagittal sinus and over the right sensorimotor cortex was significantly higher in *Vegfr3*$^{wt/wt}$ mice than *Vegfr3*$^{wt/mut}$ mice

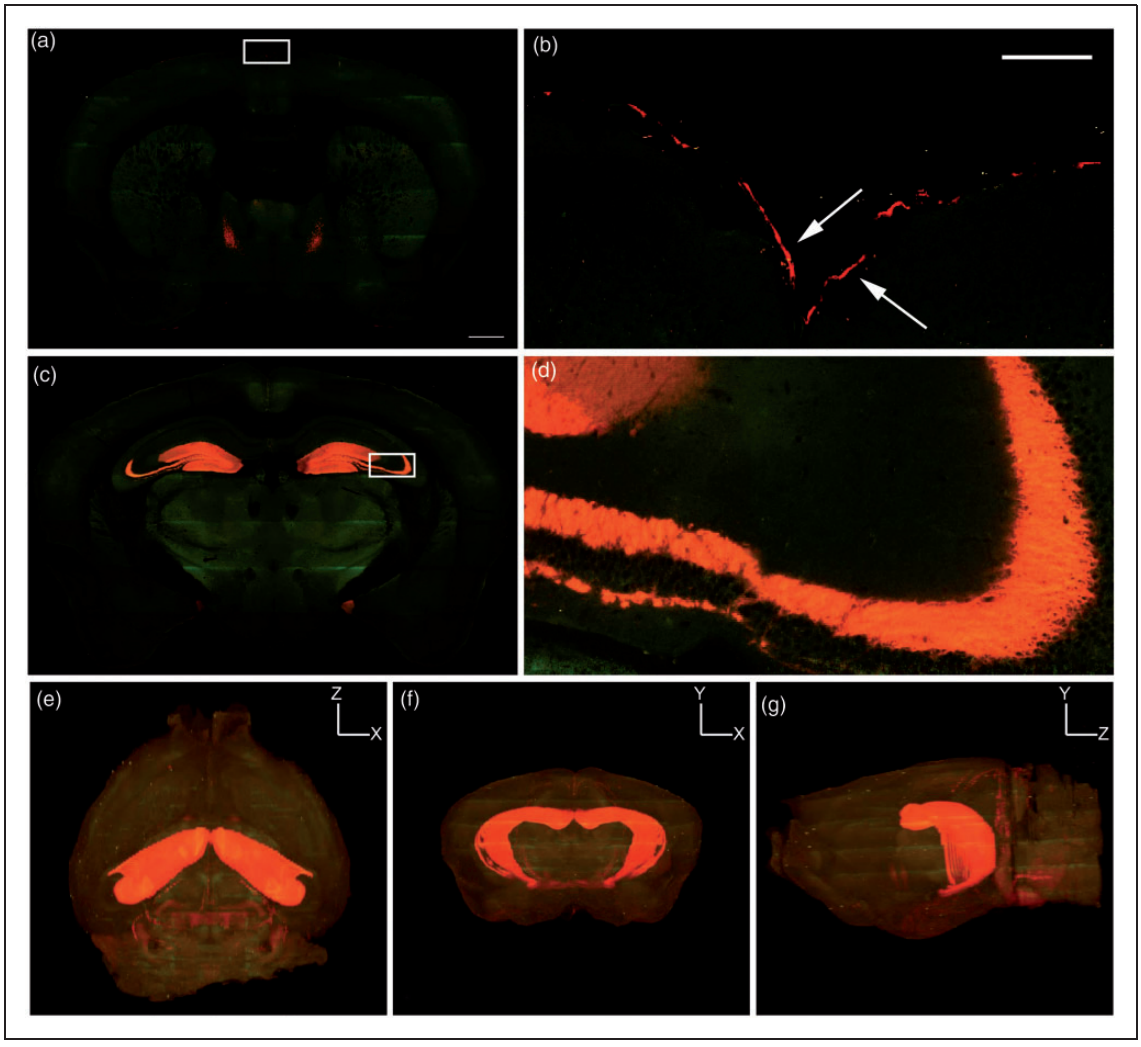

Figure 2. 3D imaging of cortical Prox-1 expression. TissueCyte serial two-photon tomography of Prox1-tdTomato (red) fluorescence shows (a–b) meningeal lymphatic expression of Prox1 near the sagittal sinus (white arrows in box enlarged from (a)) and (c–d) cytoplasmic expression within the hippocampus, with inset in (c) (white box) enlarged in (d). (e–g) 3D renderings demonstrate predominantly hippocampal cytoplasmic colocalization and no intraparenchymal lymphatic vessels. (e) Dorsal, (f) coronal and (g) sagittal views of the brain. (a,c) scale bar is 500 μm; (b,d) scale bar is 100 μm. The green color in the panels is tissue autofluorescence.

(Figure 6(b) to (d)), confirming that the meningeal lymphatic network in *Vegfr3*$^{wt/mut}$ mice remains hypoplastic after PT. There was no relationship between meningeal LVI at the sagittal sinus and infarct volume in *Vegfr3*$^{wt/wt}$. However, there was a correlation for higher meningeal LVIs to the right of the sagittal sinus in mice with more severe ischemic injury (Figure 6(e)).

Because meningeal LVs transport CSF from the ventricles to the cervical lymph nodes,[2,4] we also hypothesized that meningeal lymphatic hypoplasia could impact ventricle volume. After establishing that lateral ventricle volumes did not differ in sham *Vegfr3*$^{wt/wt}$ and *Vegfr3*$^{wt/mut}$ mice (Supplementary Figure 1(a)), we measured lateral ventricle volumes two weeks after PT. Ventricle volumes in the ischemic and uninjured hemisphere were not significantly different between *Vegfr3*$^{wt/wt}$ and *Vegfr3*$^{wt/mut}$ cohorts (Supplementary Figure 1(b)), nor was there a correlation between infarct volume and ventricle volume in (Figure 6(f) and (g)). Finally, we examined functional recovery using the rotarod behavioral task which tests motor coordination. Overall, there was no significant difference in motor skill acquisition between *Vegfr3*$^{wt/wt}$ and *Vegfr3*$^{wt/mut}$ mice after 11 days of rotarod training (Supplementary Figure 2(a)). Additionally, motor function was not significantly different between *Vegfr3*$^{wt/wt}$ and *Vegfr3*$^{wt/mut}$ mice at any of the time points examined after stroke (Supplementary Figure 2(b)). Therefore, while meningeal lymphatic hypoplasia does not affect overall infarct and lateral ventricle volume or

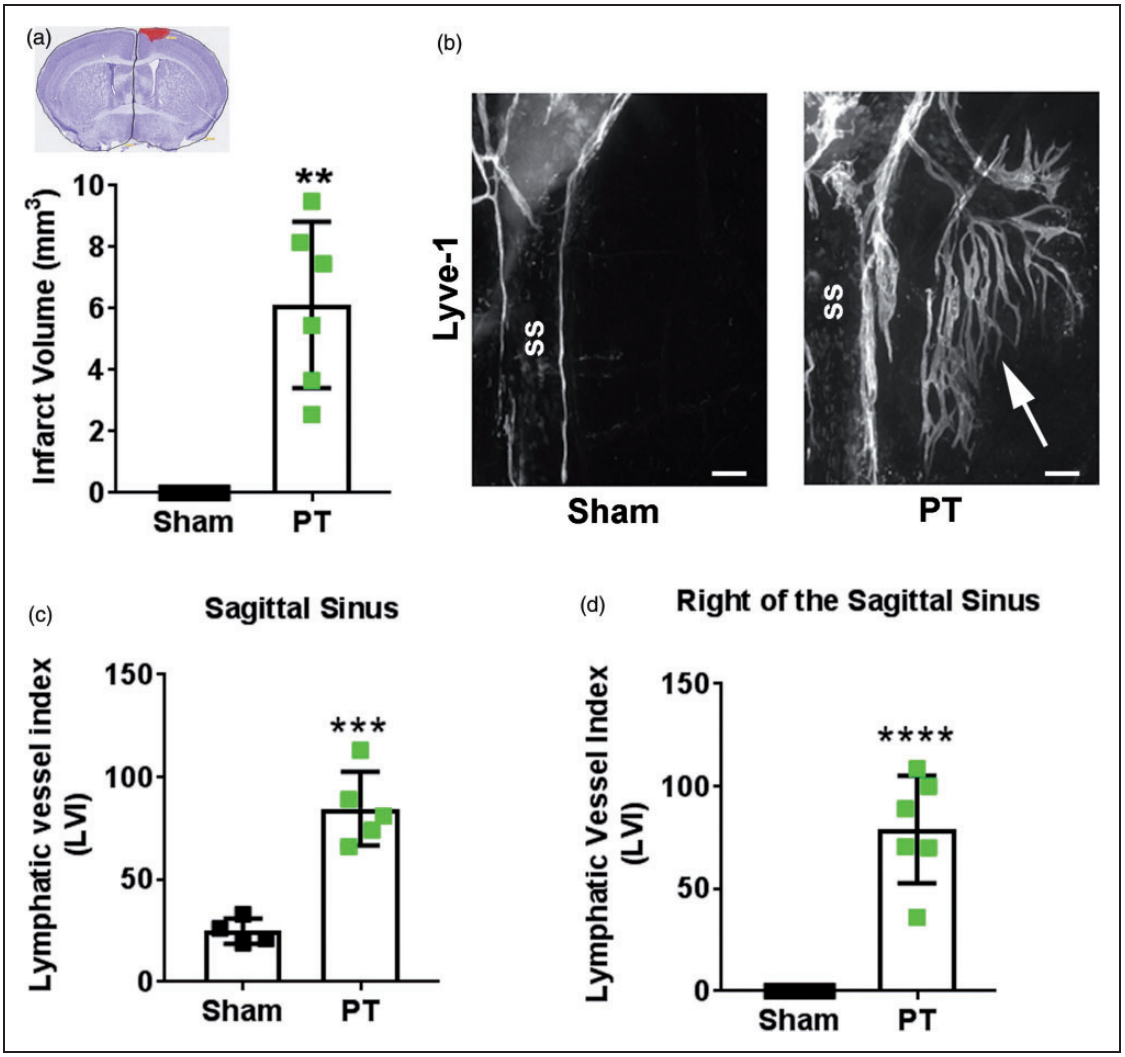

Figure 3. Photothrombosis induces meningeal lymphangiogenesis. (a) Infarct volumes in mice that received photothrombosis (PT; green squares; $n = 6$) compared to uninjured sham mice (black squares; $n = 4$). Inset shows representative cresyl violet-stained cortical section with infarct highlighted in red. (b) Representative image of lymphangiogenesis into the right sagittal sinus (ss) after PT (white arrow). (c) Quantification of meningeal lymphatic vessels at the sagittal sinus and (d) to the right of the sagittal sinus two weeks after PT stroke ($n = 5$-6) or after sham surgery ($n = 4$). All data presented as mean ± SD and were analyzed using a Mann–Whitney test. $^{**}p < 0.01$, $^{***}p < 0.001$, $^{****}p < 0.0001$. Scale bar = 200 μm.

motor recovery between cohorts, meningeal lymphangiogenesis increases in relation to PT-induced infarction in wild-type mice.

Meningeal lymphatic hypoplasia exacerbates stroke severity after tMCAo

To determine whether meningeal lymphatic hypoplasia affected the severity of stroke after tMCAo, we measured infarct volumes in *Vegfr3*$^{wt/wt}$ and *Vegfr3*$^{wt/mut}$ mice. *Vegfr3*$^{wt/mut}$ mice had significantly larger infarct volumes ($24.3 \pm 12.2\,mm^3$) than *Vegfr3*$^{wt/wt}$ mice ($9.7 \pm 6.9\,mm^3$; $p < 0.05$; Figure 7(a)) two weeks after tMCAo. The meningeal LVI at the sagittal sinus was significantly higher in *Vegfr3*$^{wt/wt}$ mice than *Vegfr3*$^{wt/mut}$ mice, but again with no meningeal lymphangiogenesis to the right of the sagittal sinus (Figure 7(b) to (d)). *Vegfr3*$^{wt/wt}$ mice exhibiting the highest LVI concomitantly had the lowest infarct volumes (Figure 7(e)). While the lateral ventricles did not differ between *Vegfr3*$^{wt/mut}$ mice than *Vegfr3*$^{wt/wt}$ mice in the ischemic hemispheres (Supplementary Figure 3), *Vegfr3*$^{wt/wt}$ mice showed a strong positive correlation between infarct volume and lateral ventricle volume that was absent in mutant mice (Figure 7(f) and (g)). Motor function was also not significantly different between *Vegfr3*$^{wt/wt}$ and *Vegfr3*$^{wt/mut}$ cohorts post-tMCAo, but *Vegfr3*$^{wt/mut}$ did exhibit sustained motor deficits

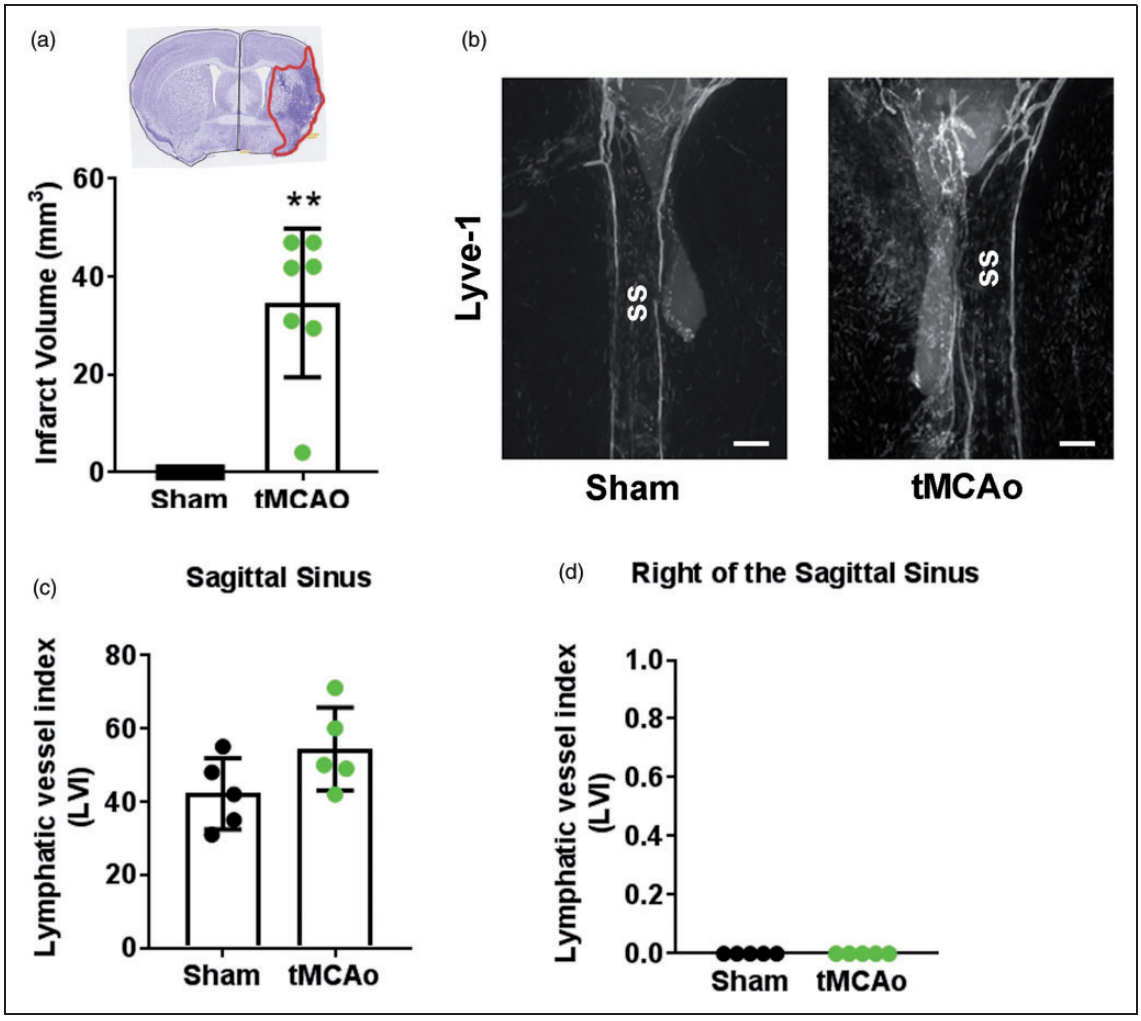

Figure 4. tMCAo does not induce meningeal lymphangiogenesis. (a) Infarct volumes in mice that received a transient middle cerebral artery occlusion (tMCAo; green circles; $n = 7$) compared to uninjured sham mice (black circles; $n = 5$). Inset shows representative cresyl violet-stained cortical section with infarct highlighted in red (b) Representative image of LVs at the sagittal sinus (ss). (c) Quantification of meningeal lymphatic vessels at the sagittal sinus ($p = 0.11$) and (d) to the right of the sagittal sinus ($p > 0.99$) two weeks after tMCAo ($n = 5$) or after sham surgery ($n = 5$). All data presented as mean ± SD and were analyzed using a Mann–Whitney test. $^{**}p < 0.01$. Scale ba = 200 μm.

throughout the two-week period (Supplementary Figure 2(c)).

Discussion

Recent interest in meningeal lymphatics has sparked many questions concerning the role of the lymphatic system in brain disease and injury. New evidence shows that the movement of macromolecules and immune cells from the CSF into meningeal LVs occurs within minutes, with Lyve-1 antibody injected into the cisterna magna covering 60% of meningeal LVs within 1 h after injection.[4] This rapid fluid movement from CSF→ meningeal LVs→ deep cervical lymph nodes (dCLN) has profound implications for both long-term neuroinflammatory diseases (e.g. multiple sclerosis (MS)), as well as acute brain injury (e.g. stroke). Direct vascular channels, also recently identified, connect the skull bone marrow to meningeal blood vessels, presenting a new route for immune cell origination and migration after stroke.[27] While meningeal LV anatomy is better understood, the functional role(s) of meningeal LVs appears to depend on the CNS disease. For example, ablation of meningeal LVs worsens pathology in a mouse model of Alzheimer's disease,[28] but reduces pathology during experimental autoimmune encephalomyelitis (EAE), a mouse model of MS.[4] As little is known about the formation and function of meningeal LVs during stroke recovery, we investigated the development and relevance of new post-stroke LVs during long-term recovery. We determined that post-stroke meningeal lymphangiogenesis is

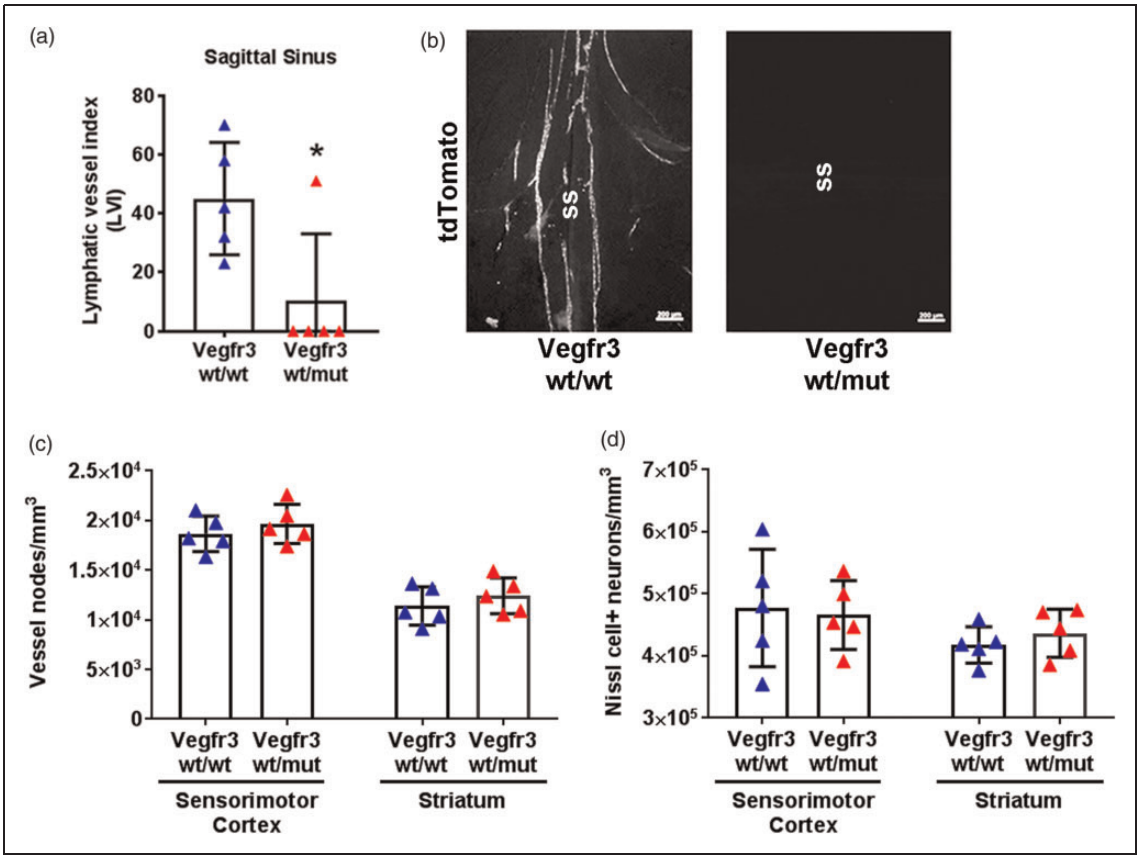

Figure 5. Meningeal hypoplasia does not affect vascular or neuronal development. (a) Quantification of LVs at the sagittal sinus in naïve *Vegfr3*$^{wt/wt}$ (blue triangles) and *Vegfr3*$^{wt/mut}$ mice (red triangles) demonstrate meningeal lymphatic hypoplasia. (b) Representative images of tdTomato+vessels at the sagittal sinus (ss). (c) Stereological quantification of microvessel density in the sensorimotor cortex ($p = 0.55$) and striatum ($p = 0.42$) of *Vegfr3*$^{wt/wt}$ and *Vegfr3*$^{wt/mut}$ mice and (d) stereological quantification of neuronal counts in the sensorimotor cortex ($p > 0.99$) and striatum ($p = 0.55$) ($n = 5$ per group). All data presented as mean ± SD and were analyzed using a Mann–Whitney test or two-way ANOVA. *$p < 0.05$. Scale bar = 200 μm.

dependent upon the method of ischemic infarction and does not occur after one the most commonly used preclinical stroke models, tMCAo. However, lymphatic hypoplasia in *Vegfr3*$^{wt/mut}$ mice exacerbates injury after tMCAo, suggesting that lymphatics play a role in stroke recovery even in the absence of overt meningeal lymphangiogenesis.

Following stroke, only PT-induced ischemic injury stimulated the sprouting of meningeal LVs into the alymphatic zone to the right of the sagittal sinus, a phenomenon not identified during EAE.[4] We hypothesize that this PT-specific lymphangiogenesis could be induced by two major factors: meningeal ischemia and stroke severity. Rose Bengal, a photosensitive dye used for PT stroke induction, also circulates in meningeal blood vessels after injection. Because the laser light passes through the meninges before reaching the cortex, photocoagulation could damage endothelial cells in the meninges, causing small vessel occlusion and possibly meningeal ischemia. In fact, qualitative assessment of meningeal CD31$^+$ blood vessels shows concomitant PT-induced angiogenesis not identified after tMCAo (Supplementary Figure 4). Meningeal ischemic injury, in turn, could stimulate compensatory lymphangiogenesis. In contrast, tMCAo induction does not include direct meningeal blood vessel occlusion. Therefore, we would not expect meningeal ischemia-induced lymphangiogenesis after tMCAo, as observed. Furthermore, the close proximity of the PT neocortical lesion to the meninges may directly induce meningeal LV sprouting through diffusion of growth factors and cytokines (e.g. VEGF, ephrins, angiopoietins)[29] from the injured neocortex to the adjacent meninges. In this case, larger injuries would stimulate more lymphangiogenesis, as shown by the positive correlation between LVI to the right of the sagittal sinus and infarct volume after PT. Lymphangiogenesis may ultimately serve to reduce neocortical edema, as occurs adjacent to ischemic injury after myocardial infarction (MI) where stimulating lymphangiogenesis after MI reduces edema and improves cardiac function.[30]

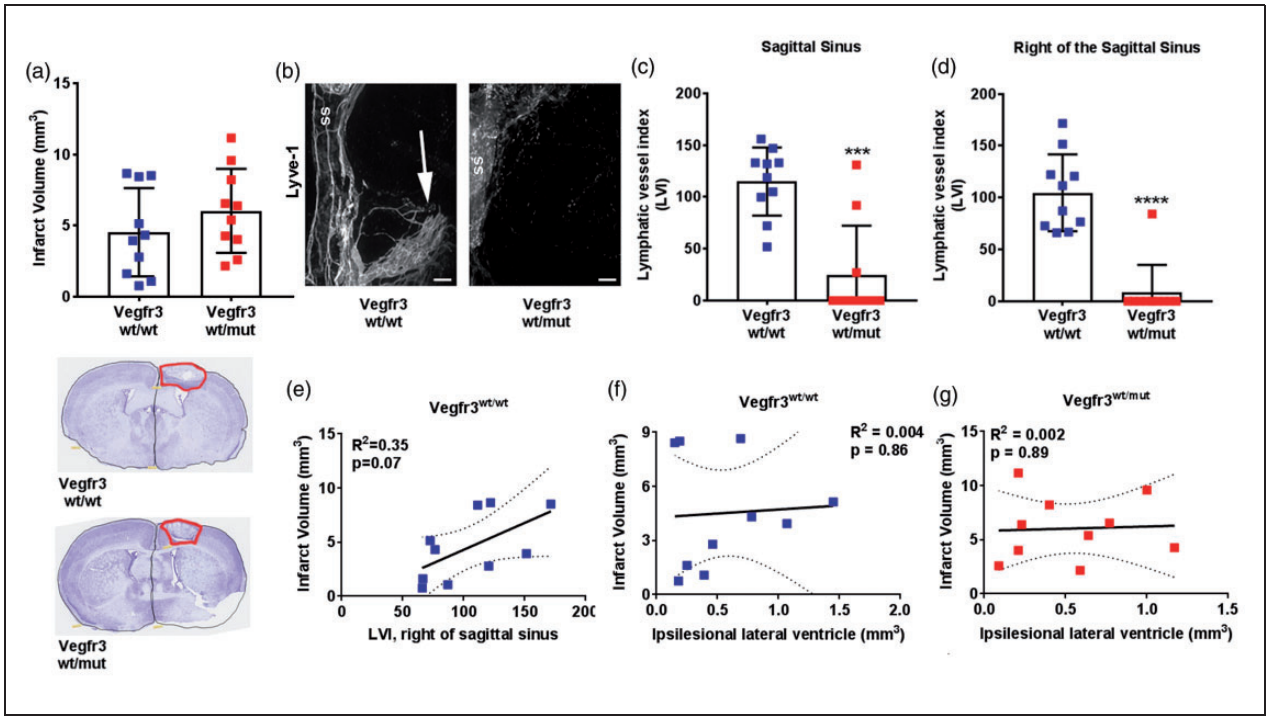

Figure 6. Photothrombosis-induced meningeal lymphangiogenesis correlates to severity of injury. (a) Quantification of infarct volumes of Vegfr3$^{wt/wt}$ (blue squares) and Vegfr3$^{wt/mut}$ (red squares) two weeks following PT ($n = 10$ per group, $p = 0.18$). Insets below graph show representative cresyl violet-stained cortical sections with infarcts highlighted in red. (b) Representative images of Lyve-1 + LVs at the sagittal sinus (ss) and right of the sagittal sinus (white arrow). (c) Quantification of meningeal LVs at the sagittal sinus and (d) to the right of the sagittal sinus of *Vegfr3*$^{wt/wt}$ and *Vegfr3*$^{wt/mut}$ ($n = 10$ per group). (e) Lymphangiogenesis correlates with increased infarct volume in *Vegfr3*$^{wt/wt}$ mice. (f,g) Linear regression of ipsilesional lateral ventricle volumes to infarct volume two weeks following PT shows no correlation in (f) *Vegfr3*$^{wt/wt}$ mice ($R^2 = 0.004$) or (G) *Vegr3*$^{wt/mut}$ ($R^2 = 0.002$). Meningeal LVI and infarct volumes were analyzed using a Mann–Whitney test or linear regression. All data presented as mean ± SD. ***$p < 0.001$, ****$p < 0.0001$. Scale bar = 200 μm.

While tMCAo did not induce meningeal lymphangiogenesis, sham tMCAo mice did exhibit a larger LVI compared to sham PT mice, possible representing a general dilation of the meningeal LVs at the sagittal sinus secondary to permanent CCA ligation. Dilation of LVs increases drainage under high pressure conditions,[31] particularly relevant after stroke as edema increases intracranial pressure and infarct volumes, worsening stroke outcomes.[32] But LV dilation also improves delivery of lymph to the draining lymph nodes, which modulates neuroinflammation during EAE.[33] Under homeostatic conditions, meningeal LVs transport immune cells, such as T cells, to the dCLN where they encounter antigen and become activated.[2,4] As stroke induces the release of brain-derived antigens[13] that quickly spread from the CSF to the meningeal LVs,[4] it is critical in future experiments to understand the contribution of meningeal LVs to the early adaptive – and potentially beneficial – autoimmune responses in both mice[13] and humans.[34] While our data suggest that higher meningeal LVI is associated with lower infarction after tMCAo, this could be a methodological artifact and thus needs to be confirmed with intravital microscopy or specific meningeal LV ablation.[4]

VEGFR3 signaling is required for the development and maintenance of meningeal LVs in mice,[5] and multiple stroke models show that VEGF-C and VEGFR3 expression is upregulated following tMCAo.[35,36] Inhibition of VEGFR3 blocks ischemic preconditioning-induced tolerance against transient ischemic injury, implicating this pathway in neuroprotection.[37] We found that mice with a point mutation that disrupts VEGFR3 signaling (*Vegfr3*$^{wt/mut}$ mice) have a hypoplastic network of meningeal LVs. We also found that *Vegfr3*$^{wt/mut}$ mice had significantly larger infarct volumes than *Vegfr3*$^{wt/wt}$ mice after tMCAo, but not after PT-induced stroke. The tMCAo model induces a greater magnitude of neurovascular injury versus PT. While PT strokes are limited largely to the sensorimotor cortex, tMCAos result in larger infarcts that involve the striatum, cortex, and in some cases the thalamus, hippocampus, and subventricular zone.[38] Mice also exhibit larger penumbras and greater edema after

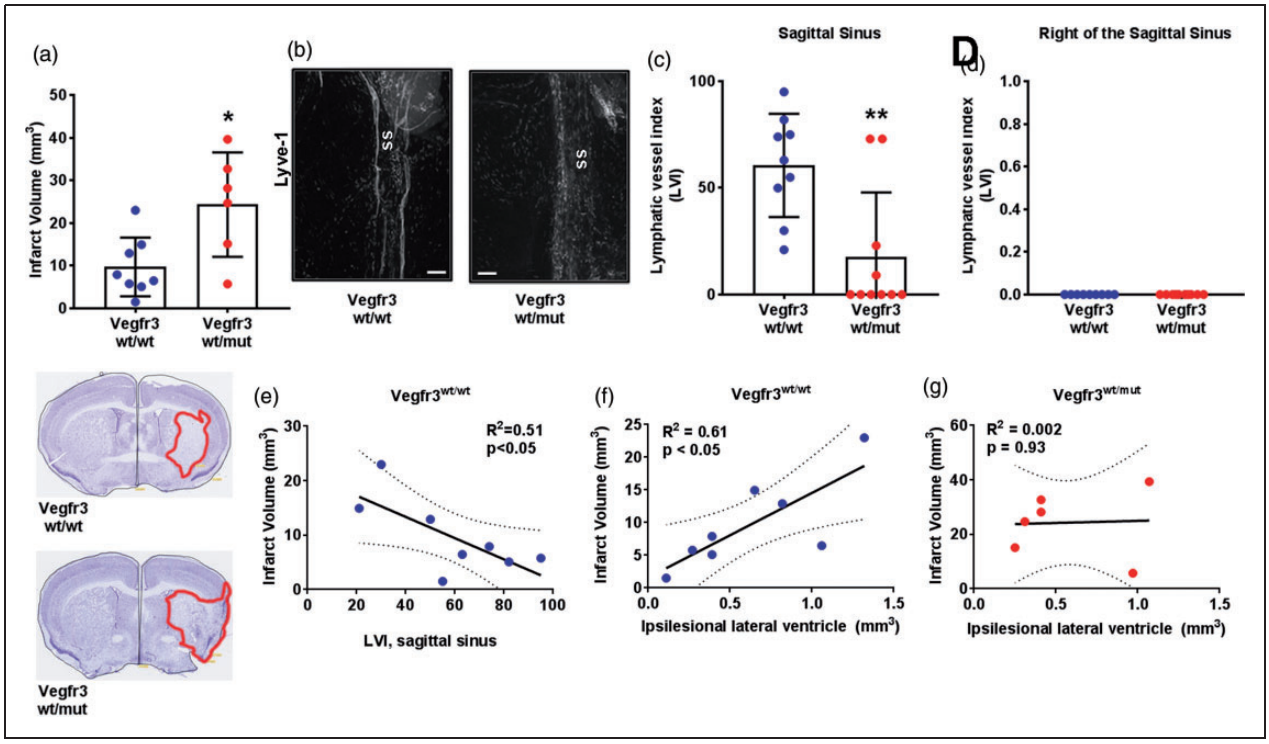

Figure 7. Meningeal lymphatic hypoplasia increases infarct volumes after tMCAo. (a) Quantification of infarct volumes of *Vegfr3*$^{wt/wt}$ (blue circles) and *Vegfr3*$^{wt/mut}$ (red circles) mice two weeks following transient middle cerebral artery occlusion (tMCAo; $n = 6$–8 per group). Insets below graph show representative cresyl violet-stained cortical sections with infarcts highlighted in red. (b) Representative images of Lyve-1 + LVs at the sagittal sinus (ss). (c) Quantification of meningeal LVs at the sagittal sinus and (d) to the right of the sagittal sinus ($p > 0.99$) of *Vegfr3*$^{wt/wt}$ and *Vegfr3*$^{wt/mut}$ mice ($n = 9$–10 per group). (e) Sagittal sinus LVI correlates with decreased infarct volume in *Vegfr3*$^{wt/wt}$ mice. (f) Increased infarct volumes correlate with increased ipsilesional ventricle volumes in *Vegfr3*$^{wt/wt}$ ($R^2 = 0.61$) but not in (g) *Vegr3*$^{wt/mut}$ ($R^2 = 0.002$) mice. Meningeal LVI and infarct volumes were analyzed using a Mann–Whitney test and linear regression. All data presented as mean ± SD. *$p < 0.05$, **$p < 0.01$. Scale bar = 200 μm.

tMCAo.[32,39] Therefore, a stronger injury/stressor such as tMCAo may be required to reveal the importance of meningeal LVs after stroke. Finally, in the clinic, stroke patients in general have enlarged ventricles compared to healthy elderly controls.[40,41] Researchers attribute this increased ventricular volume to brain atrophy and the loss of white matter, providing evidence to support our correlation between infarct severity and larger lateral ventricle volume after tMCAo in *Vegfr3*$^{wt/wt}$ mice. But what should be investigated in future studies is how critical potential meningeal LV dilation is for ventricular volume and infarction, especially considering the rapid movement between these fluid compartments.[4] Together, these data suggest the importance of meningeal lymphatic drainage of CSF after stroke, possibly including additional ventral meningeal LVs not isolated and analyzed in our whole-mount protocol.

Overall, our study is the first to demonstrate that ischemia impacts meningeal LVs after stroke, and that these meningeal LVs are important for stroke outcome. Using two common models of ischemic stroke, tMCAo and PT, we found that only one type of stroke – PT – induced meningeal lymphangiogenesis. tMCAo, however, was a severe stressor that revealed that meningeal lymphatic hypoplasia exacerbated stroke severity. Our findings reveal novel differences between the PT and tMCAo models of stroke and underscore the need to use multiple stroke models in future studies investigating the role of meningeal LVs in CNS disease.

Acknowledgements

We thank the UT Southwestern Whole Brain Microscopy Facility (WBMF) in the department of Neurology and Neurotherapeutics for assistance with serial two-photon tomography. We would also like to acknowledge the contributions of the UT Southwestern Neuromodels Facility for PT and tMCAo surgeries and post-operative care. The C3H101H-Flt4^{Chy}/H (VEGFR3) mice were obtained from the MRC Harwell which distributes this strain on behalf of the European Mouse Mutant Archive (EMMA: www.infrafrontier.eu). The repository number is EM:00068. The C3H101H-Flt4^{Chy}/H (VEGFR3) mice were originally generated at the MRC-Harwell.

Authors' contributions

PY, KP, MTD, and AMS designed the studies, interpreted data, and drafted the manuscript; PY, KP, DH, NK, KRZ, MB, EJP, MTD, and AMS executed experiments and analyzed data. All authors revised and approved the final submission.

Funding

The author(s) disclosed receipt of the following financial support for the research, authorship, and/or publication of this article: This study was funded by grants to A.M.S. from the American Heart Association (14SDG18410020), NIH/NINDS (NS088555), the Dana Foundation (David Mahoney Neuroimaging grant), and The Haggerty Center for Brain Injury and Repair (UTSW). The WBMF is supported by the Texas Institute for Brain Injury and Repair (TIBIR).

Declaration of conflicting interests

The author(s) declared no potential conflicts of interest with respect to the research, authorship, and/or publication of this article.

Supplementary material

Supplementary material for this paper can be found at the journal website: http://journals.sagepub.com/home/jcb

References

1. Witte MH, Way DL, Witte CL, et al. Lymphangiogenesis: mechanisms, significance and clinical implications. *EXS* 1997; 79: 65–112.
2. Louveau A, Smirnov I, Keyes TJ, et al. Structural and functional features of central nervous system lymphatic vessels. *Nature* 2015; 523: 337–341.
3. Aspelund A, Antila S, Proulx ST, et al. A dural lymphatic vascular system that drains brain interstitial fluid and macromolecules. *J Exp Med* 2015; 212: 991–999.
4. Louveau A, Herz J, Alme MN, et al. CNS lymphatic drainage and neuroinflammation are regulated by meningeal lymphatic vasculature. *Nat Neurosci* 2018; 21: 1380–1391.
5. Antila S, Karaman S, Nurmi H, et al. Development and plasticity of meningeal lymphatic vessels. *J Exp Med* 2017; 214: 3645–3667.
6. Karkkainen MJ, Saaristo A, Jussila L, et al. A model for gene therapy of human hereditary lymphedema. *Proc Natl Acad Sci U S A* 2001; 98: 12677–12682.
7. Joukov V, Pajusola K, Kaipainen A, et al. A novel vascular endothelial growth factor, VEGF-C, is a ligand for the Flt4 (VEGFR-3) and KDR (VEGFR-2) receptor tyrosine kinases. *EMBO J* 1996; 15: 1751.
8. Achen MG, Jeltsch M, Kukk E, et al. Vascular endothelial growth factor D (VEGF-D) is a ligand for the tyrosine kinases VEGF receptor 2 (Flk1) and VEGF receptor 3 (Flt4). *Proc Natl Acad Sci U S A* 1998; 95: 548–553.
9. Gu W, Brannstrom T, Jiang W, et al. Vascular endothelial growth factor-A and -C protein up-regulation and early angiogenesis in a rat photothrombotic ring stroke model with spontaneous reperfusion. *Acta Neuropathol* 2001; 102: 216–226.
10. Si J, Chen L and Xia Z. Effects of cervical-lymphatic blockade on brain edema and infarction volume in cerebral ischemic rats. *Chin J Physiol* 2006; 49: 258–265.
11. Selvaraj UM, Ortega SB, Hu R, et al. Preconditioning-induced CXCL12 upregulation minimizes leukocyte infiltration after stroke in ischemia-tolerant mice. *J Cereb Blood Flow Metab* 2017; 37: 801–813.
12. Lane-Donovan C, Desai C, Pohlkamp T, et al. Physiologic Reelin does not play a strong role in protection against acute stroke. *J Cereb Blood Flow Metab* 2016; 36: 1295–1303.
13. Ortega SB, Noorbhai I, Poinsatte K, et al. Stroke induces a rapid adaptive autoimmune response to novel neuronal antigens. *Discov Med* 2015; 19: 381–392.
14. Stowe AM, Adair-Kirk TL, Gonzales ER, et al. Neutrophil elastase and neurovascular injury following focal stroke and reperfusion. *Neurobiol Dis* 2009; 35: 82–90.
15. Ragan T, Kadiri LR, Venkataraju KU, et al. Serial two-photon tomography for automated ex vivo mouse brain imaging. *Nat Methods* 2012; 9: 255–258.
16. Hamming AM, Wermer MJ, Umesh Rudrapatna S, et al. Spreading depolarizations increase delayed brain injury in a rat model of subarachnoid hemorrhage. *J Cereb Blood Flow Metab* 2016; 36: 1224–1231.
17. Gidday JM, Gasche YG, Copin JC, et al. Leukocyte-derived matrix metalloproteinase-9 mediates blood-brain barrier breakdown and is proinflammatory after transient focal cerebral ischemia. *Am J Physiol Heart Circ Physiol* 2005; 289: H558–H568.
18. Miller BA, Perez RS, Shah AR, et al. Cerebral protection by hypoxic preconditioning in a murine model of focal ischemia-reperfusion. *Neuroreport* 2001; 12: 1663–1669.
19. West MJ and Gundersen HJ. Unbiased stereological estimation of the number of neurons in the human hippocampus. *J Comp Neurol* 1990; 296: 1–22.
20. Løkkegaard A. The number of microvessels estimated by an unbiased stereological method applied in a brain region. In: Evans SM, Janson AM and Nyengaard JR (eds) *Quantitative Methods in Neuroscience: A Neuroanatomical Approach*. Oxford: OUP, 2004, pp.167–182.
21. Hominick D, Silva A, Khurana N, et al. VEGF-C promotes the development of lymphatics in bone and bone loss. *Elife* 2018; 7: 1–22.
22. Baluk P, Fuxe J, Hashizume H, et al. Functionally specialized junctions between endothelial cells of lymphatic vessels. *J Exp Med* 2007; 204: 2349–2362.
23. Banerji S, Ni J, Wang SX, et al. LYVE-1, a new homologue of the CD44 glycoprotein, is a lymph-specific receptor for hyaluronan. *J Cell Biol* 1999; 144: 789–801.
24. Wigle JT and Oliver G. Prox1 function is required for the development of the murine lymphatic system. *Cell* 1999; 98: 769–778.
25. Kriehuber E, Breiteneder-Geleff S, Groeger M, et al. Isolation and characterization of dermal lymphatic and

blood endothelial cells reveal stable and functionally specialized cell lineages. *J Exp Med* 2001; 194: 797–808.
26. Karlsen TV, Karkkainen MJ, Alitalo K, et al. Transcapillary fluid balance consequences of missing initial lymphatics studied in a mouse model of primary lymphoedema. *J Physiol* 2006; 574: 583–596.
27. Herisson F, Frodermann V, Courties G, et al. Direct vascular channels connect skull bone marrow and the brain surface enabling myeloid cell migration. *Nat Neurosci* 2018; 21: 1209–1217.
28. Wen YR, Yang JH, Wang X, et al. Induced dural lymphangiogenesis facilities soluble amyloid-beta clearance from brain in a transgenic mouse model of Alzheimer's disease. *Neural Regen Res* 2018; 13: 709–716.
29. Coso S, Bovay E and Petrova TV. Pressing the right buttons: signaling in lymphangiogenesis. *Blood* 2014; 123: 2614–2624.
30. Vieira JM, Norman S, Villa Del Campo C, et al. The cardiac lymphatic system stimulates resolution of inflammation following myocardial infarction. *J Clin Invest* 2018; 128: 3402–3412.
31. Quick CM, Venugopal AM, Gashev AA, et al. Intrinsic pump-conduit behavior of lymphangions. *Am J Physiol Regul Integr Comp Physiol* 2007; 292: R1510–R1518.
32. Ropper AH and Shafran B. Brain edema after stroke. Clinical syndrome and intracranial pressure. *Arch Neurol* 1984; 41: 26–29.
33. Liao S, Cheng G, Conner DA, et al. Impaired lymphatic contraction associated with immunosuppression. *Proc Natl Acad Sci U S A* 2011; 108: 18784–18789.
34. Planas AM, Gomez-Choco M, Urra X, et al. Brain-derived antigens in lymphoid tissue of patients with acute stroke. *J Immunol* 2012; 188: 2156–2163.
35. Shin YJ, Choi JS, Choi JY, et al. Induction of vascular endothelial growth factor receptor-3 mRNA in glial cells following focal cerebral ischemia in rats. *J Neuroimmunol* 2010; 229: 81–90.
36. Shin YJ, Park JM, Cho JM, et al. Induction of vascular endothelial growth factor receptor-3 expression in perivascular cells of the ischemic core following focal cerebral ischemia in rats. *Acta Histochem* 2013; 115: 170–177.
37. Bhuiyan MI, Kim JC, Hwang SN, et al. Ischemic tolerance is associated with VEGF-C and VEGFR-3 signaling in the mouse hippocampus. *Neuroscience* 2015; 290: 90–102.
38. Fluri F, Schuhmann MK and Kleinschnitz C. Animal models of ischemic stroke and their application in clinical research. *Drug Des Devel Ther* 2015; 9: 3445–3454.
39. Beard DJ, Logan CL, McLeod DD, et al. Ischemic penumbra as a trigger for intracranial pressure rise – a potential cause for collateral failure and infarct progression? *J Cereb Blood Flow Metab* 2016; 36: 917–927.
40. Lenzi GL, Padovani A, Di Piero V, et al. White matter changes and ventricular enlargement on magnetic resonance imaging: comparison between normal elderly subjects and patients with cerebrovascular disorders. *J Stroke Cerebrovasc Dis* 1994; 4: 245–249.
41. Padovani A, Di Piero V, Bragoni M, et al. Correlates of leukoaraiosis and ventricular enlargement on magnetic resonance imaging: a study in normal elderly and cerebrovascular patients. *Eur J Neurol* 1997; 4: 15–23.